Mechanical and Electromagnetic Properties of Self-Compacted Geopolymer Concretes With Nano Silica and Steel Fiber Additives

Ugur Cem Hasar, *Member, IEEE*, Necip Altay Eren, Hamdullah Ozturk, Mucahit Izginli, Huseyin Korkmaz, Abdulkadir Cevik, Anil Nis, and Mohammad R. Irshidat

***Abstract*— Mechanical and electromagnetic properties (over 2–16 GHz) of self-compacted geopolymer concrete (SCGC) samples with different amounts of nanosilica (NS) and steel-fiber (SF) have been examined. From the mechanical tests, it is observed that, while the amount of NS added to SCGC samples does not make any noticeable change in compressive strength and modulus of elasticity values, an increase in the amount and/or aspect ratio of SF additives improves these values. From the electromagnetic tests, it is noted that the effect of SF on the reflection properties of SCGC samples is relatively smaller than the effect of NS. Besides, while the incorporation of NS improves the resonance characteristics of transmission properties, additives of SF decrease these properties over the entire frequency band. Finally, sample C7, which has 1% SF with a smaller diameter and 2% NS in reference to the mass of the binder, has the optimum NS and SF additives, producing maximum absorbance values.**

***Index Terms*— Concrete, electromagnetic properties, geopolymer, mechanical properties, nanosilica (NS), self-compact, steel fiber (SF).**

I. Introduction

ELECTROMAGNETIC signals have widespread usage in industrial manufacture, wireless communication, and military applications. Production of high-frequency electronic equipments and household appliances, as well as ever-growing wireless communication technology, have increased the risks of electromagnetic signals on human being, such as nerve system [1] and hormone profiles [2]. To eliminate or suppress the aforementioned risks of electromagnetic signals, electromagnetic shielding can be applied by weakening electromagnetic signals across a material or a structure [3]–[9].

Metallic structures are the best and natural electromagnetic shielding materials; however, their metallic corrosion effect, complex and expensive fabrication process, and high density prevent them from being used directly within cement-based structures [9], [10]. Besides, cement-based structures generally have a lower electromagnetic shielding effectiveness. For example, reflection loss of an ordinary gravel is around −5 dB [4]. To improve the shielding effectiveness and reduce the electromagnetic interference of cement-based materials (CBMs), various nanomaterial additives producing dielectric and/or magnetic loss have been applied, including graphene oxide, TiO_2 powder, Fe_3O_4 powder, Mn–Zn powder, silica fume, carbon black, nanocarbontube, carbon filament and carbon fiber, fly ash, ferrite powder, boron ores, and rubber [4]–[18].

CBMs have widespread usage in the construction industry. However, their brittleness limits their application for areas in which severe earthquakes are possible to happen and in which long-term service lives play a critical role. On the other hand, engineered cementitious composites (ECCs) are a special kind of fiber reinforced CBMs [19] to meet the demand for construction areas prone to strong earthquakes because these composites have high ductility compared with CBMs. Besides, ECCs are unique composites having high tensile and flexural strengths thanks to the fiber that interacts with cement matrix, resulting in crack size minimization [20]. Various studies have been performed on analysis of their mechanical [21], micromechanism [22], and thermal [23] properties. In addition mechanical properties, electromagnetic properties of ECCs has been established recently [24]–[28].

The ordinary Portland cement (OPC) has been commonly used as a binder for concrete structures. However, the manufacture of cement is costly because it necessitates a high amount of temperature. A recent study has revealed that Portland cement production contributes to approximately 7% of total CO_2 in the world [29]. As a new form of concrete, geopolymer concretes do not require OPC as a binder [30] and, thus, are considered an environmentally friendly concrete. In general, geopolymer concrete has good mechanical properties (gaining strength at early ages), resistance to acids and sulfates, and low creep and shrinkage [31]. The utilization of geopolymer concrete also reduces the consumption of industrial waste and by-products in addition to the reduction of CO_2 emissions [32]. Besides, self-compacting geopolymer concrete (SCGC) is considered one of the latest developments in concrete technology with the advantage of no vibration requirement for putting and placing. In this study, we examine

Manuscript received November 30, 2021; revised March 7, 2022; accepted April 2, 2022. Date of publication May 9, 2022; date of current version May 23, 2022. This work was supported in part by the Scientific Research Projects Coordination Unit of Gaziantep University under Project MF.DT.17.06. The Associate Editor coordinating the review process was Dr. Christoph Baer. *(Corresponding author: Ugur Cem Hasar.)*

Ugur Cem Hasar, Hamdullah Ozturk, and Huseyin Korkmaz are with the Department of Electrical and Electronics Engineering, Gaziantep University, 27310 Gaziantep, Turkey (e-mail: uchasar@gantep.edu.tr).

Necip Altay Eren and Abdulkadir Cevik are with the Department of Civil Engineering, Gaziantep University, 27310 Gaziantep, Turkey.

Mucahit Izginli is with the Department of Electrical and Electronics Engineering, Hasan Kalyoncu University, 27410 Gaziantep, Turkey.

Anil Nis is with the Department of Civil Engineering, Istanbul Gelisim University, 34315 Istanbul, Turkey.

Mohammad R. Irshidat is with the Center for Advanced Materials, Qatar University, Doha, Qatar.

Digital Object Identifier 10.1109/TIM.2022.3173272

the electromagnetic shielding effectiveness of SCGC with various nanosilica (NS) and steel-fiber (SF) additives.

II. Materials

A. Raw Materials and Mixture Proportions

Slag is a by-product of iron production in iron and steel plants. Granulated slag showing a pozzolanic feature—called ground granulated blast furnace slag (GGBFS)—is produced when the iron blast furnace slag is suddenly cooled down. At least 66% of the GGBFS's mass consists of calcium oxide, magnesium oxide, and silicon dioxide. The NS, which is a highly pozzolanic material with fine particles (100 nm) much less than the particles of an ordinary cement (approximately 1000 times smaller), manufactured by aerosol was purchased from the company Chemtrec in the USA. The SFs in hooked-end shape with different amounts were used in the fabrication of concretes. While crushed limestone with a grain size varying between 5 and 11 mm was used as the coarse aggregate, crushed sand with a grain size smaller than 4 mm was utilized as the fine aggregate.

Some chemical admixtures, such as superplasticizers (SPs), could be utilized to improve workability and prevent the disintegration of particles. In our study, polycarboxylates ether was applied as SPs with a specific gravity of 1.1 kg/m^3 and a density of 1.095 g/cm^3. Besides, a mixture of Na_2SiO_3 and NaOH operated as the alkaline solution was prepared in our laboratory before one day of concreting. Na_2SiO_3 has the ingredient, by mass, of 13.7% Na_2SiO, 29.4% SiO_2, and 56.9% water, which was purchased from a local supplier (ZAG Kimya) in Gaziantep, Turkey. NaOH pellets were purchased from Kosflake Company with a purity of 98% $\mp$ 0.5. Fig. 1(a)–(e) illustrates photographs of GGBFS, NS, SF, SP, and NaOH solution obtained from NaOH pellets. Table I demonstrates the chemical composition and physical properties, such as the ignition loss, the specific gravity, and the Blaine fineness, which affects the hydration rate (setting) and the requirements for the amounts of water, retarder, and dispersant, of GGBFS and NS [33]. SFs have the same diameter of 0.75 mm, the aspect ratio of 40/80, and the relative density of 7840 kg/m^3 but different lengths of 30 (denoted by "SF-1") and 60 mm (denoted by "SF-2").

B. Mixing Procedure and Sample Preparation

Ten different mixes with a constant binder content and value of 500 kg/m^3 were prepared to examine the mechanical and electromagnetic properties (reflection, transmission, and absorption) of SCGC. In preparation of each SCGC, first, NaOH solution was obtained by dissolving NaOH pellets in water. The optimum concentration for mechanical properties of SCGC was achieved by dissolving these pellets in 12 molar concentration of NaOH [34]. Next, Na_2SiO_3 and NaOH solutions (with Na_2SiO_3 to NaOH ratio of 2.5 [35]) were mixed for approximately 24 h to activate the prepared alkaline solution before casting. Then, SP and extra water were sequentially added in 1-min intervals after adding the prepared alkaline solution. After, they were swiftly and continuously mixed for

Fig. 1. Photographs of (a) GGBFS, (b) NS, (c) SP, (d) SF, and (e) NaOH [33].

TABLE I
Chemical Composition and Physical Properties of the GGBFS and NS

Chemical composition (%)	GGBFS	NS
CaO	34.12	–
SiO_2	36.40	99.80
Al_2O_3	11.39	–
Fe_2O_3	1.69	–
MgO	10.30	–
SO_3	0.49	–
K_2O	3.63	–
Na_2O	0.35	–
Physical properties		
Ignition loss (m^2/kg)	1.64	<1.00
Specific gravity (g/cm^3)	2.79	2.20
Blaine fineness (m^2/kg)	418	–

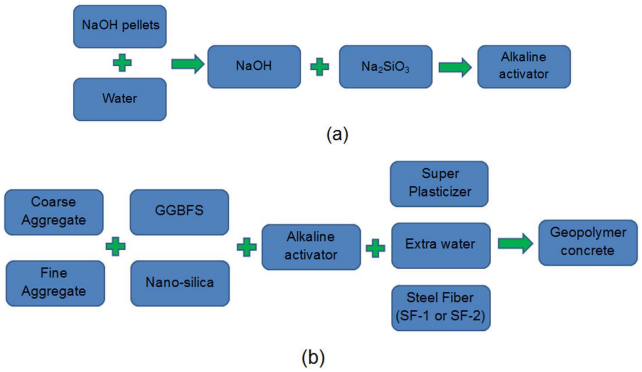

Fig. 2. Procedures for preparing (a) alkaline activator and (b) SCGC [33].

2 min. Thereafter, SF was added to some mixtures, and the fresh mixture was mixed for an additional 3 min to ensure homogeneity throughout the mixture. NS was added into some SCGC samples with a ratio of 2% by weight of the binder. SF was also included in SCGC samples with the ratios of 0.5% and 1.0%. Fig. 2(a) and (b) shows the procedures for preparing alkaline activator and SCGC [33]. Mixture proportions of the prepared SCGC samples with different NS and SF additives are presented in Table II. For each mix, Na_2SO_3 + NaOH solution, molarity, percentage of SP, and percentage of extra water were set to 250 kg/m^3, 12, 7, and 10, respectively.

III. Measurement Procedures for Mechanical and Electromagnetic Tests

A. Measurement Procedure for Mechanical Tests

After casting three sets of SCGC samples in the form of a cube ($100 \times 100 \times 100$ mm^3) for tests of compressive strength

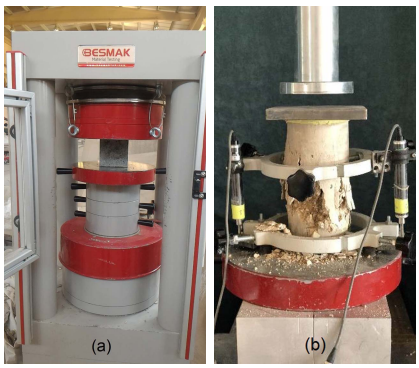

Fig. 3. Photographs of testing machines for (a) compressive strength measurements [26] and (b) modulus of elasticity [33].

TABLE II
SAMPLE LABELS AND THEIR MIXTURE INGREDIENTS OF SCGC [33]

Mix.	Binder (kg/m^3)	GGBFS (kg/m^3)	NS (kg/m^3)	SF (kg/m^3)	F. Aggr. (kg/m^3)	C. Aggr. (kg/m^3)
C1	500	500	0	0	860.07	738.12
C2	500	500	0	39.2*	860.07	738.12
C3	500	500	0	78.4*	860.07	738.12
C4	500	500	0	39.2**	860.07	738.12
C5	500	500	0	78.4**	860.07	738.12
C10	500	490	10	0	858.49	736.76
C6	500	490	10	39.2*	858.49	736.76
C7	500	490	10	78.4*	858.49	736.76
C8	500	490	10	39.2**	858.49	736.76
C9	500	490	10	78.4**	858.49	736.76

Here, '$\star$' and '$\star\star$' refer, respectively, to SF-1 and SF-2, and 'F. Aggr.' and 'C. Aggr.' denote fine and coarse aggregates, respectively.

and in the form of a cylinder (ϕ100 $\times$ 200 mm) for tests of modulus of elasticity with different NS and SF additives, they were demolded after 24 h and placed in the ambient environment for 28 days. Compressive strength tests of samples were carried out using the built-in hydraulic compressive strength testing machine purchased from BesMak (with the maximum continuous loading capacity of 3000 kN) [26], as shown in Fig. 3(a). On the other hand, modulus of elasticity tests was conducted by a compress meter containing a dial gauge capable of measuring deformation down to 0.002 mm by the measuring machine shown in Fig. 3(b). The samples were loaded three times to 40% of the ultimate load, which was determined using compressive strength test results.

B. Measurement Procedure for Electromagnetic Tests

Additional SCGC samples with transverse dimensions of 500 $\times$ 500 mm^2 and lengths of approximately 60 mm were prepared for measuring their free-space electromagnetic properties (reflection, transmission, and absorption) by using a constructed measurement setup, as shown in Fig. 4. Different from the free-space measurement setup based on an arching reflection method in the study [36], our measurement setup, similar to those in the studies [11], [15]–[18], [37], is useful for measuring both reflection and transmission properties of prepared SCGC samples with different NS and SF additives. It includes a vector network analyzer (VNA) instrument, two horn antennas, and two coaxial-line cables [37]–[39]. The VNA instrument (Keysight Instruments with model N9918A)

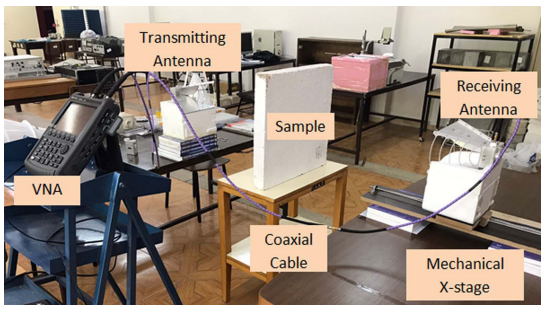

Fig. 4. Photo of the measurement setup used for measuring electromagnetic properties (reflection, transmission, and absorption) of SCGC samples with different NS and SF additives.

generates electromagnetic signals and measures forward and backward reflection scattering (S-)parameters (S_{11} and S_{22}) and forward and backward transmission S-parameters (S_{21} and S_{12}) of SCGC samples over the frequency range between 30 kHz and 26.5 GHz. It has a dynamic range of 90 dB for a frequency range up to 18 GHz and a directivity greater than 32 dB over the full frequency range. Horn antennas were operated efficiently transmitting and receiving electromagnetic signals to SCGC samples. They are linearly polarized antennas purchased from the company Pasternack (PE9888-11) having a cross section of 204 $\times$ 164 mm^2 and an operating range of approximately 2–16 GHz and with a nominal gain of 11 dB and an input VSWR of 1.5, which is corrected by the calibration technique to be discussed shortly. The coaxial-line cables each having a length of approximately 200 mm are rugged phase-stable cables used for establishing a secure connection between the VNA instrument and the input of the horn antennas. Because we used the time-gating option of the VNA, to be discussed in Section IV-B, which was set around the sample region by selecting a proper time interval in the time-gating process [37] and because prepared samples had relatively larger transverse planes in square form (500 $\times$ 500 mm^2), it was observed that microwave absorbers positioned near the SCGC samples did not much improve our free-space measurements [38], [39]. For this reason, we continued our measurements without using absorbers for the sake of simplicity and easiness.

Before starting to measurements, the measurement system was calibrated using the thru-reflect-line (TRL) calibration technique [40]. This is a versatile calibration technique and especially useful for free-space measurement systems (calibrating measurement systems having genderless connections) [41]. Toward this end, while a highly reflective (without the need for knowing its reflectivity) metal plate with a transverse dimension of 500 $\times$ 500 mm^2 and a thickness of approximately 4 mm (greater than the skin depth for the frequency range of 2–16 GHz) was operated as the short standard, a free-space region of 7.89 mm, which was set by a moving the receiving antenna located on a mechanical X-stage, was utilized as the line standard. The SCGC samples were located at nearly far zones of the transmitting and receiving antennas [15], which were separated by a distance of more than 2 m. This ensures approximately plane wave propagation through the samples. On the other hand, the larger transverse

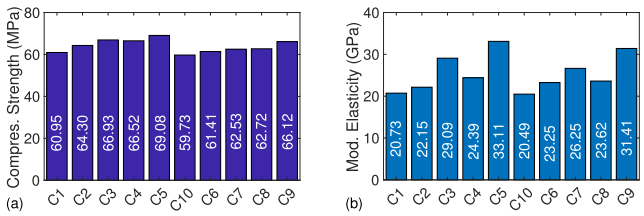

Fig. 5. (a) Compressive strength and (b) modulus of elasticity results of SCGC samples with different NS and SF for 28 days of hardened state [33].

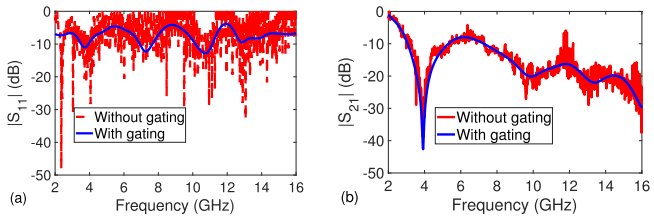

Fig. 6. Analysis of the time-domain gating effect on measured $|S_{11}|$ (dB) and $|S_{21}|$ (dB) of sample C1 over the 2–16-GHz frequency band.

dimension (500×500 mm^2) of SCGC samples removed the diffraction effects, which might appear in their corners and edges (sharp points). Finally, the time-domain gating feature of the VNA was activated to eliminate any possible reflections from the stage that the samples were located and between transmitting and receiving horn antennas [15], [28], [37]–[39].

IV. Measurement Results and Discussion

A. Results of Mechanical Properties of CSGC Samples

Fig. 5(a) illustrates the average compressive strength results of SCGC samples for the 28 days of curing. It is seen from Fig. 5(a) that the addition of NS to SCGC samples had almost no effect on the compressive strength values. However, it is observed that, as expected, an increase in the amount of SF and its aspect ratio increases the measured compressive strength values. The samples C5 and C9 have the highest compressive strength values of 69.08 and 66.12, respectively [33]. Besides, Fig. 5(b) demonstrates the average modulus of elasticity results of SCGC samples for the 28 days of curing. It is noted from Fig. 5(b) that the modulus of elasticity varies between 20.49 and 33.11 GPa for the prepared SCGC samples. Parallel with the compressive strength test results, the modulus of elasticity of SCGC samples increases with an increase in the amount and aspect ratio of SFs. As an example of the effect of SF amount, while sample C2 has the modulus of elasticity value of 22.15, sample C3 has the modulus of elasticity value of 29.09 (approximately 30% increase). As an example of the effect of SF aspect ratio, whereas sample C2 has the modulus of elasticity value of 22.15, sample C4 has the modulus of elasticity value of 24.39 (approximately 10% increase). Besides, although NS does not essentially have an effect of modulus on elasticity, it is observed from Fig. 5(b) that additive of NS to SCGC samples decreased relatively in small quantity the modulus of elasticity. For instance, while sample C5 has the modulus of elasticity value of 33.11, sample C9 has the modulus of elasticity value of 31.41 (approximately 5% decrease). We think that such a decrease can be associated with unreacted NS particles in the matrix.

B. Results of Electromagnetic Properties of CSGC Samples

Before presenting the electromagnetic properties of prepared SCGC samples, the effect of the time-domain gating was examined. Fig. 6(a) and (b) demonstrates the forward reflection $|S_{11}|$ (dB) and forward transmission $|S_{21}|$ (dB) properties of sample C1 with/out time-domain gating over the 2–16-GHz frequency band (the full frequency range of the antenna). Here, $|\star|$ denotes the magnitude of the complex quantity "$\star$." It is noted that, because backward reflection $|S_{22}|$ and backward transmission $|S_{12}|$ properties are, respectively, similar to $|S_{11}|$ and $|S_{21}|$, from now on, only the results of $|S_{11}|$ and $|S_{21}|$ will be presented for each sample for conciseness. Results are presented in dB form in lieu of absolute form [15] because such a presentation can effectively demonstrate discrepancies between measured quantities with small differences in levels. It is noted that the time-domain gating can be applied over reflection or transmission responses. In our analysis, we applied this gating over main transmission properties [41] (roughly varying from -500 ps to 1.0 ns for each sample). It is seen from Fig. 6(a) and (b) that gating eliminates ripples, which could arise from reflections from the stage (or ground) and between transmitting and receiving antennas, in reflection and transmission properties of sample C1 over the full frequency band. Besides, it is also noted from Fig. 6(a) that the gating removes some measured artifacts ($|S_{11}| > 0$ dB) [42] at some certain frequencies and, thus, corrects the measured $|S_{11}|$. Furthermore, the gating makes the resonance properties (e.g., the dip observed at approximately 4 GHz in $|S_{11}|$ and $|S_{21}|$) of sample C1 seen clearly, which are associated with collective behavior of the multiple-bouncing signals within the sample from its end faces. It should be mentioned here that, as the first disadvantage of the time-domain gating process, the isolation of ripples or superfluous signals in the frequency domain by the time-domain gating process degrades with increased frequency bandwidth [39]. As the second disadvantage, because the time-domain gating filters undesired or unwanted signals in the frequency domain by applying a suitable window function, such as rectangular (default), Hanning, and Kaiser–Bessel windows in the time domain, the recovered signal after the gating process may have some small ripples or bends at the lowest and height frequency regions of the original signal. From this point on, we will present only the results of gated reflection, transmission, and absorption properties of SCGC samples.

1) Reflection Properties: Fig. 7(a) and (b) illustrates frequency dependence of reflection properties $|S_{11}|$ of the prepared SCGC samples (C1, C2, . . . , C10) with different NS and SF additives. The following points are noted from the results in Fig. 7(a) and (b). First, when the $|S_{11}|$ values of the samples C2, C3, C4, and C5 are compared with the $|S_{11}|$ value of sample C1 in Fig. 7(a), there seems relatively smaller effect of SF on reflection properties $|S_{11}|$ of SCGC samples over 2–16-GHz frequency range. Second, the addition of NS to SCGC samples increases the interaction of electromagnetic waves with SCGC samples. For example, sample C7 has three sharp dips where

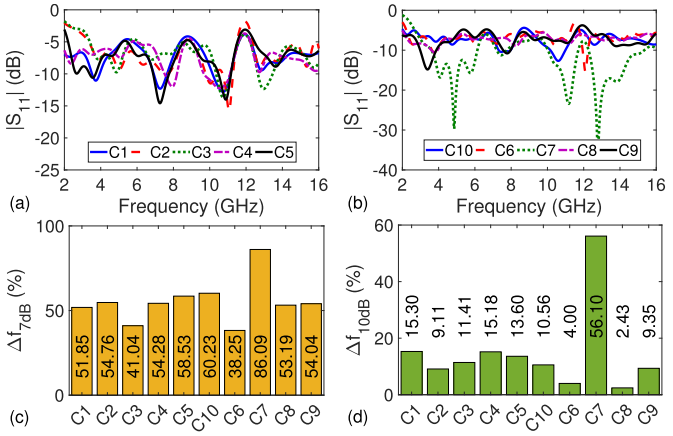

Fig. 7. Reflection properties of the prepared SCGC samples with different NS and SF additives. (a) $|S_{11}|$ values of the samples C1, C2, C3, C4, and C5 and (b) $|S_{11}|$ values of the samples C6, C7, C8, C9, and C10 over the 2–16-GHz frequency band, and (c) $\Delta f_{7\,\mathrm{dB}}$ and (d) $\Delta f_{10\,\mathrm{dB}}$ values of all samples.

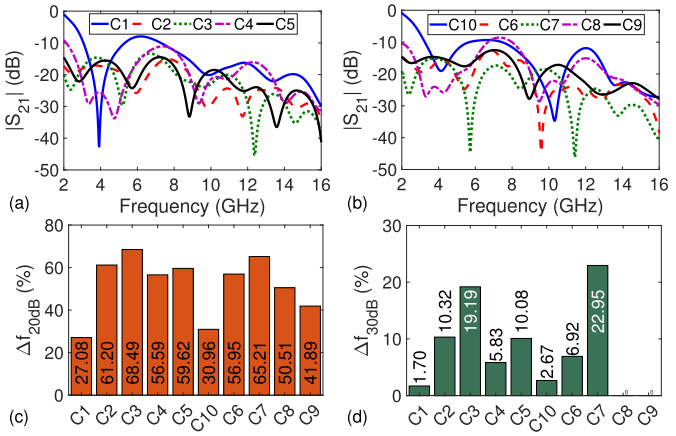

Fig. 8. Transmission properties of the prepared SCGC samples with different NS and SF additives. (a) $|S_{21}|$ values of the samples C1, C2, C3, C4, and C5 and (b) $|S_{21}|$ values of the samples C6, C7, C8, C9, and C10 over the 2–16-GHz frequency band, and (c) $\Delta f_{20\,\mathrm{dB}}$ and (d) $\Delta f_{30\,\mathrm{dB}}$ values of all samples.

$|S_{11}|$ values drop to approximately -30, -24, and -37 dB at frequencies of 4.86, 11.17, and 12.78 GHz, respectively. Third, this interaction, however, decreases for SCGC samples with a larger diameter of SF, which might demonstrate resonance behavior at lower frequencies (less than 2 GHz). It is known that a larger scatterer will demonstrate resonance behavior at lower frequencies [43].

Aside from examining minimum reflection properties $|S_{11}|$ at some frequencies, the analysis of cumulative reflection properties $|S_{11}|$ over the full frequency band is equally important for gaining more information about reflection properties of the prepared SCGC samples. To this end, in reference to a full frequency band, we analyzed the effective bandwidth Δf [28], [44], which could be utilized as a fair comparison of absorbing properties of our prepared SCGC samples with the same thickness. Two precise metrics for the effective bandwidth were utilized [44]: 1) the frequency bandwidth ($\Delta f_{10\,\mathrm{dB}}$) over which $|S_{11}|$ is less than -10 dB for military applications and 2) the frequency bandwidth ($\Delta f_{7\,\mathrm{dB}}$) over which $|S_{11}|$ is smaller than -7 dB for general-purpose applications. Fig. 7(c) and (d) illustrate the $\Delta f_{7\,\mathrm{dB}}$ (%) and $\Delta f_{10\,\mathrm{dB}}$ (%) values of prepared SCGC samples. It is seen from Fig. 7(c) and (d) that sample C7 has the highest $\Delta f_{7\,\mathrm{dB}}$ and $\Delta f_{10\,\mathrm{dB}}$ values compared with those of the remaining SCGC samples. Besides, it can be concluded within the scope of effective bandwidth that, while all prepared SCGC samples can be used for a general-purpose $|S_{11}|$ reduction (effective for $\Delta f_{7\,\mathrm{dB}}$), only sample C7 should be selected for military applications with approximately 56% value for $\Delta f_{10\,\mathrm{dB}}$ (far above the $\Delta f_{10\,\mathrm{dB}}$ values of other SCGC samples).

2) Transmission Properties: In addition to reflection properties $|S_{11}|$, we also measured transmission properties $|S_{21}|$ of all prepared SCGC samples (C1, C2, ..., C10). Fig. 8(a) and (b) demonstrates the frequency dependencies of $|S_{21}|$. The following remarks are noted from the dependencies in Fig. 8(a) and (b). First, different from the effect of SF on $|S_{11}|$, additives of SF reduce the value of $|S_{21}|$, meaning that SF prevents electromagnetic signals from passing through the SCGC samples. For example, the $|S_{21}|$ value (dB) of sample C1 is, in general, greater than those of the samples C2, C3, C4, and C5, except for the frequency around 4 GHz. On the other hand, sample C3 has the lowest $|S_{21}|$ value (approximately -46 dB) at nearly 12.4 GHz. Second, similar to the point made in the analysis of reflection properties $|S_{11}|$, the addition of NS to SCGC samples with SF having a smaller diameter improves the interaction of electromagnetic signals. For instance, while sample C3 has one dip value around 12.4 GHz, sample C7 has two dip values around 5.73 (-44.57) and 11.42 GHz (-46.1 dB). Besides, whereas sample C2 has no $|S_{21}|$ value less than -40 dB, sample C6 has a $|S_{21}|$ value of -44.7 dB at 9.6 GHz.

Parallel with the definition of effective bandwidths (-7 and -10 dB) for reflection properties, we also determined effective bandwidths for transmission properties. However, in lieu of -7- and -10-dB values for effective bandwidths for reflection properties, we considered -20 dB ($\Delta f_{20\,\mathrm{dB}}$) and -30 dB ($\Delta f_{30\,\mathrm{dB}}$) values for effective bandwidths for transmission properties to better evaluate the wave attenuation performance of the prepared SCGC samples. Fig. 8(c) and (d) shows $\Delta f_{20\,\mathrm{dB}}$ and $\Delta f_{20\,\mathrm{dB}}$ values. It is observed from Fig. 8(c) that the addition of SF to SCGC samples, in general, increases $\Delta f_{20\,\mathrm{dB}}$ due to the well-known absorption capability of SF [45]. Specifically, the SF brings SCGC samples in microwave absorption capability around -7 dB. On the other hand, when the $\Delta f_{20\,\mathrm{dB}}$ values in Fig. 8(d) are compared, it is seen that the SCGC samples with SF additives having smaller diameter (30 mm) interacts with electromagnetic signals more than the SCGC samples with SF additives having a larger diameter (60 mm). Additionally, effect of NS deteriorates $\Delta f_{30\,\mathrm{dB}}$ values except for sample C7, which has the maximum $f_{30\,\mathrm{dB}}$ value of 22.95%.

3) Absorption Properties: In addition to reflection and transmission properties, absorption properties of prepared SCGC samples are also important because these properties can demonstrate the ability to absorb electromagnetic signals. Absorption properties of a sample can be written as [15]

$$A = 1 - R - T \tag{1}$$

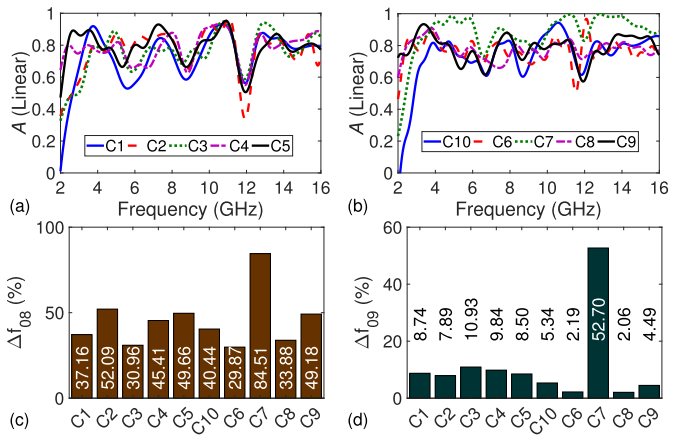

Fig. 9. Absorption properties of the prepared SCGC samples with different NS and SF additives. (a) A values of the samples C1, C2, C3, C4, and C5 and (b) A values of the samples C6, C7, C8, C9, and C10 over the 2–16-GHz frequency band, and (c) Δf_{08} and (d) Δf_{09} values of all samples.

where $R = |S_{11}|^2$ and $T = |S_{21}|^2$ denote, respectively, the reflectivity and the transmittivity. It is seen from (1) that the values of R and T should approach zero in order to get maximum absorption by the sample.

The expressions of $|S_{11}|$ and $|S_{21}|$ of a flat sample (with infinite transverse area) surrounded by free-space can be written [43] as

$$|S_{11}| = \left|\frac{\Gamma(1-P^2)}{1-\Gamma^2 P^2}\right|, \quad |S_{21}| = \left|\frac{P(1-\Gamma^2)}{1-\Gamma^2 P^2}\right| \tag{2}$$

where Γ is the interfacial reflection coefficient and P is the propagation factor within the sample. Their expressions are

$$\Gamma = \frac{z-1}{z+1}, \quad P = e^{-jk_0 nd}, \quad z = \sqrt{\frac{\mu_r}{\varepsilon_r}}, \quad n = \sqrt{\mu_r \varepsilon_r} \tag{3}$$

where z and n are the normalized intrinsic impedance and the refractive index of the sample; d is the sample length; μ_r and ε_r are the relative permeability and permittivity of the sample; $k_0 = \omega/c$ is the free-space wavenumber; $\omega = 2\pi f$ is the angular frequency; c is the velocity of light in vacuum (approximately air); and f is the linear frequency.

It is noted from Fig. 8(a) and (b) that $|S_{21}|$ of all prepared SCGC samples are smaller than -10 dB. Then, we can consider these samples as high-loss samples ($P^2 \to 0$) [43], [46] and approximate $|S_{11}|$ and $|S_{21}|$ in (2) to

$$|S_{11}|_{\text{approx}} = |\Gamma|, \quad |S_{21}|_{\text{approx}} = |P(1-\Gamma^2)|. \tag{4}$$

Therefore, maximum A can be achieved if $|\Gamma|$ approaches zero, which can be realized when $\mu_r \cong \epsilon_r$, for high-loss samples with a small $|P|$ value. An identical result is also utilized for metal-backed (shorted) samples [15], [28], [45], [47].

Fig. 9(a) and (b) illustrates the frequency dependence of A of the prepared SCGC samples. It is noted from Fig. 9(a) and (b) that all samples have lower A values at frequencies lower than approximately 4 GHz. Especially, the samples C1 and C10 behave as transparent materials below 4 GHz, which can be attributed to no SF content. Beyond this frequency, their absorption capabilities demonstrate few oscillations, which we think are partly due to relatively smaller internal multiple reflections and are partly due to the cables, in general above 0.6 except for some discrete frequencies, such as 5.9 and 12 GHz. Besides, sample C7 has A values approaching unity (approximately 0.996) at specific frequencies of 11.17 and 12.75 GHz. To gain more information about the absorption capabilities of the prepared SCGC samples, we evaluated the effective bandwidths Δf_{08} and Δf_{09}, which corresponds to the frequency bandwidths, when A is greater than the value of 0.8 and 0.9, respectively. The calculated Δf_{08} and Δf_{09} values are demonstrated in Fig. 9(c) and (d). It is noted from the results in Fig. 9(c) and (d) that sample C2 has better Δf_{08} and Δf_{09} metric values than those of sample C6. Besides, it is clearly seen from Fig. 9(c) and (d) that sample C7 has the maximum Δf_{08} and Δf_{09} values (far greater than those of the remaining samples). This means that, in terms of the absorption capabilities of the prepared SCGC samples, one can conclude that sample C7 has the optimum NS and SF additives.

In our current study, we presented only $|S_{11}|$ and $|S_{21}|$ [and then calculated A from (1)] of SCGC samples because measured phases of S_{11} and S_{21} include some errors due partly to the insufficient accuracy of the X-band stage in our present measurement setup. In near future, we want to improve the accuracy of phase measurements by our setup. Besides, in this study, electromagnetic reflection, transmission, and absorbance properties of SCGC samples with different NS and SF additives have been measured (along with their discussions). As future studies, we want to conduct studies on the same properties of SCGC samples with different additives, such as graphene oxide, TiO2 powder, Fe3O4 powder, Mn–Zn powder, silica fume, carbon black, nanocarbontube, carbon filament and carbon fiber, fly ash, ferrite powder, boron ores, and waste tire rubber.

V. Conclusion

Various SCGC samples with different NS and SF additives were prepared, and their mechanical (compressive strength and modulus of elasticity) and electromagnetic (reflection, transmission, and absorption properties) properties were measured. The following main results are noted from mechanical tests. First, the amount of NS added to SCGC samples does not make any noticeable change in compressive strength and modulus of elasticity values. Second, a small amount of decrease in modulus of elasticity after NS addition to SCGC samples arises mainly due to unreacted NS particles in the matrix. Third, an increase in the amount and/or aspect ratio of SF additives improves both the compressive strength and the modulus of elasticity values of SCGC samples. Fourth, NS additive does not essentially have an effect on the modulus of elasticity. The following main results are observed from electromagnetic measurements. First, the effect of SF on $|S_{11}|$ measurements of SCGC samples is relatively smaller than the effect of NS on the same measurements. Second, within the scope of effective bandwidth, it can be said that, while all prepared SCGC samples can be used for a general-purpose

$|S_{11}|$ reduction, sample C7 can be used for general-purpose and military applications. Third, while additives of SF decrease the values of $|S_{21}|$ (attenuation), the addition of NS improves the resonance characteristics of $|S_{21}|$. Fourth, while all prepared SCGC samples have smaller absorbance for frequencies lower than 4 GHz, sample C7 has absorbance values approaching unity (approximately 0.996) at specific frequencies of 11.17 and 12.75 GHz. Finally, incorporation of SF to SCGC samples in general (except for sample C2) improves the absorption capabilities of SCGC samples, and sample C7 has the optimum NS and SF additives, producing maximum Δf_{08} and Δf_{09} values.

REFERENCES

[1] L. G. Salford *et al.*, "The mammalian brain in the electromagnetic fields designed by man with special reference to blood-brain barrier function, neuronal damage and possible physical mechanisms," *Prog. Theor. Phys. Suppl.*, vol. 173, pp. 283–309, 2008.

[2] E. F. Eskander, S. F. Estefan, and A. A. Abd-Rabou, "How does long term exposure to base stations and mobile phones affect human hormone profiles?" *Clin. Biochem.*, vol. 45, nos. 1–2, pp. 157–161, Jan. 2012.

[3] Y. He, L. Lu, K. Sun, F. Wang, and S. Hu, "Electromagnetic wave absorbing cement-based composite using nano-Fe_3O_4 magnetic fluid as absorber," *Cement Concrete Compos.*, vol. 92, pp. 1–6, Sep. 2018.

[4] L. Lu, Y. He, B. Ping, F. Wang, and S. Hu, "TiO_2 containing electromagnetic wave absorbing aggregate and its application in concrete," *Construct. Building Mater.*, vol. 134, pp. 602–609, Mar. 2017.

[5] M. Cakir, N. U. Kockal, S. Ozen, A. Kocakusak, and S. Helhel, "Investigation of electromagnetic shielding and absorbing capabilities of cementitious composites with waste metallic chips," *J. Microw. Power Electromagn. Energy*, vol. 51, no. 1, pp. 31–42, Jan. 2017.

[6] H. Guan, S. Liu, Y. Duan, and J. Cheng, "Cement based electromagnetic shielding and absorbing building materials," *Cement Concrete Compos.*, vol. 28, no. 5, pp. 468–474, May 2006.

[7] H. Guan, S. Liu, Y. Duan, and Y. Zhao, "Investigation of the electromagnetic characteristics of cement based composites filled with EPS," *Cement Concrete Compos.*, vol. 29, no. 1, pp. 49–54, Jan. 2007.

[8] X. Liu, J. Wu, J. He, and L. Zhang, "Electromagnetic interference shielding effectiveness of titanium carbide sheets," *Mater. Lett.*, vol. 205, pp. 261–263, Oct. 2017.

[9] A. P. Singh, M. Mishra, A. Chandra, and S. K. Dhawan, "Graphene oxide/ferrofluid/cement composites for electromagnetic interference shielding application," *Nanotechnology*, vol. 22, no. 46, Oct. 2011, Art. no. 465701.

[10] P. Saini, V. Choudhary, B. Singh, R. Mathur, and S. Dhawan, "Polyaniline–MWCNT nanocomposites for microwave absorption and EMI shielding," *Mater. Chem. Phys.*, vol. 113, no. 2, pp. 919–926, 2009.

[11] M. Ozturk, O. Akgol, U. K. Sevim, M. Karaaslan, M. Demirci, and E. Unal, "Experimental work on mechanical, electromagnetic and microwave shielding effectiveness properties of mortar containing electric arc furnace slag," *Construct. Building Mater.*, vol. 165, pp. 58–63, Mar. 2018.

[12] J. Chen, D. Zhao, H. Ge, and J. Wang, "Graphene oxide-deposited carbon fiber/cement composites for electromagnetic interference shielding application," *Construct. Building Mater.*, vol. 84, pp. 66–72, Jun. 2015.

[13] I. W. Nam, H. K. Kim, and H. K. Lee, "Influence of silica fume additions on electromagnetic interference shielding effectiveness of multi-walled carbon nanotube/cement composites," *Construct. Building Mater.*, vol. 30, pp. 480–487, May 2012.

[14] Y. Dai, M. Sun, C. Liu, and Z. Li, "Electromagnetic wave absorbing characteristics of carbon black cement-based composites," *Cement Concrete Compos.*, vol. 32, no. 7, pp. 508–513, Aug. 2010.

[15] M. Ozturk, M. Karaaslan, O. Akgol, and U. K. Sevim, "Mechanical and electromagnetic performance of cement based composites containing different replacement levels of ground granulated blast furnace slag, fly ash, silica fume and Rice husk ash," *Cement Concrete Res.*, vol. 136, Oct. 2020, Art. no. 106177.

[16] M. Ozturk, T. Depci, E. Bahceci, M. Karaaslan, O. Akgol, and U. K. Sevim, "Production of new electromagnetic wave shielder mortar using waste mill scales," *Construct. Building Mater.*, vol. 242, May 2020, Art. no. 118028.

[17] M. Ozturk, U. K. Sevim, O. Akgol, E. Unal, and M. Karaaslan, "Investigation of the mechanic, electromagnetic characteristics and shielding effectiveness of concrete with boron ores and boron containing wastes," *Construct. Building Mater.*, vol. 252, Aug. 2020, Art. no. 119058.

[18] M. Ozturk, T. Depci, M. Karaaslan, U. K. Sevim, O. Akgol, and S. O. Hacioglu, "Synergetic effect of waste tire rubber and mil scale on electromagnetic wave attenuation properties of new generation mortar," *J. Building Eng.*, vol. 30, Jul. 2020, Art. no. 101249.

[19] V. C. Li, "On engineered cementitious composites (ECC): A review of the material and its applications," *J. Adv. Concrete Technol.*, vol. 1, no. 5, pp. 215–230, 2003.

[20] H. Ma, S. Qian, and Z. Zhang, "Effect of self-healing on water permeability and mechanical property of medium-early-strength engineered cementitious composites," *Construct. Building Mater.*, vol. 68, pp. 92–101, Oct. 2014.

[21] B.-T. Huang, Q.-H. Li, S.-L. Xu, and B.-M. Zhou, "Frequency effect on the compressive fatigue behavior of ultrahigh toughness cementitious composites: Experimental study and probabilistic analysis," *J. Struct. Eng.*, vol. 143, no. 8, Aug. 2017, Art. no. 04017073.

[22] Q. Li, X. Gao, and S. Xu, "Multiple effects of nano-SiO_2 and hybrid fibers on properties of high toughness fiber reinforced cementitious composites with high-volume fly ash," *Cement Concrete Compos.*, vol. 72, pp. 201–212, Sep. 2016.

[23] Q.-H. Li, C.-J. Sun, and S.-L. Xu, "Thermal and mechanical properties of ultrahigh toughness cementitious composite with hybrid PVA and steel fibers at elevated temperatures," *Compos. B, Eng.*, vol. 176, Nov. 2019, Art. no. 107201.

[24] K. Chung, C. Zhang, Y. Li, L. Sun, and M. Ghannam, "Microwave nondestructive inspection and prediction of modulus of rupture and modulus of elasticity of engineered cementitious composites (ECCs) using dual-frequency correlation," *Sensors*, vol. 17, no. 12, p. 2831, Dec. 2017.

[25] K. L. Chung *et al.*, "Strength prediction and correlation of cement composites: A cross-disciplinary approach," *IEEE Access*, vol. 7, pp. 41746–41756, 2019.

[26] U. C. Hasar, F. Bozdag, M. Bute, H. Ozturk, and A. Cevik, "Sample placement effect during curing on microwave reflection properties of early age engineered cementitious mortar specimens," *IEEE Trans. Instrum. Meas.*, vol. 69, no. 8, pp. 5763–5771, Aug. 2020.

[27] U. C. Hasar, M. Izginli, H. Ozturk, H. Korkmaz, A. Cevik, and M. R. Irshidat, "Surface curing effect on reflection response of hardened cementitious mortar samples," *Measurement*, vol. 185, Nov. 2021, Art. no. 110026.

[28] Y. Shen, Q. Li, S. Xu, and X. Liu, "Electromagnetic wave absorption of multifunctional cementitious composites incorporating polyvinyl alcohol (PVA) fibers and fly ash: Effects of microstructure and hydration," *Cement Concrete Res.*, vol. 143, May 2021, Art. no. 106389.

[29] C. Chen, G. Habert, Y. Bouzidi, and A. Jullien, "Environmental impact of cement production: Detail of the different processes and cement plant variability evaluation," *J. Cleaner Prod.*, vol. 18, no. 5, pp. 478–485, 2010.

[30] J. Davidovits, "Geopolymers and geopolymeric materials," *J. Thermal Anal.*, vol. 35, no. 2, pp. 1633–1656, 1991.

[31] J. Davidovits, "Global warming impact on the cement and aggregates industries," *World Resour. Rev.*, vol. 6, no. 2, pp. 263–278, 1994.

[32] D. Hardjito, S. E. Wallah, D. M. J. Sumajouw, and B. V. Rangan, "On the development of fly ash-based geopolymer concrete," *ACI Mater. J.*, vol. 101, no. 6, pp. 467–472, 2004.

[33] N. A. Eren, "Behavior of geopolymer concrete under impact," Ph.D. dissertation, Dept. Civil Eng., Gaziantep Univ., Gaziantep, Turkey, Jul. 2021.

[34] F. A. Memon, M. F. Nuruddin, S. Khan, N. A. S. I. R. Shafiq, and T. Ayub, "Effect of sodium hydroxide concentration on fresh properties and compressive strength of selfcompacting geopolymer concrete," *J. Eng. Sci. Technol.*, vol. 8, no. 1, pp. 44–56, 2013.

[35] M. Olivia and H. Nikraz, "Properties of fly ash geopolymer concrete designed by Taguchi method," *Mater. Des.*, vol. 36, pp. 191–198, Apr. 2012.

[36] S. Xie, Z. Ji, B. Li, L. Zhu, and J. Wang, "Electromagnetic wave absorption properties of helical carbon fibers and expanded glass beads filled cement-based composites," *Compos. A, Appl. Sci. Manuf.*, vol. 114, pp. 360–367, Nov. 2018.

[37] U. C. Hasar *et al.*, "Improved method for permittivity determination of dielectric samples by free-space measurements," *IEEE Trans. Instrum. Meas.*, vol. 71, pp. 1–8, 2022.

[38] U. C. Hasar, G. Ozturk, Y. Kaya, and M. Ertugrul, "Calibration-free time-domain free-space permittivity extraction technique," *IEEE Trans. Antennas Propag.*, vol. 70, no. 2, pp. 1565–1568, Feb. 2022.

[39] U. C. Hasar *et al.*, "Complex permittivity and thickness evaluation of low-loss dielectrics from uncalibrated free-space time-domain measurements," *IEEE Trans. Geosci. Remote Sens.*, vol. 60, pp. 1–10, 2022.
[40] G. F. Engen and C. A. Hoer, "Thru-reflect-line: An improved technique for calibrating the dual six-port automatic network analyzer," *IEEE Trans. Microw. Theory Techn.*, vol. MTT-27, no. 12, pp. 987–993, Dec. 1979.
[41] D. K. Ghodgaonkar, V. V. Varadan, and V. K. Varadan, "Free-space measurement of complex permittivity and complex permeability of magnetic materials at microwave frequencies," *IEEE Trans. Instrum. Meas.*, vol. 39, no. 2, pp. 387–394, Apr. 1990.
[42] U. C. Hasar, Y. Kaya, J. J. Barroso, and M. Ertugrul, "Determination of reference-plane invariant, thickness-independent, and broadband constitutive parameters of thin materials," *IEEE Trans. Microw. Theory Techn.*, vol. 63, no. 7, pp. 2313–2321, Jul. 2015.
[43] U. C. Hasar, "Non-destructive testing of hardened cement specimens at microwave frequencies using a simple free-space method," *NDT E Int.*, vol. 42, no. 6, pp. 550–557, Sep. 2009.
[44] B. Zhao *et al.*, "Yolk–Shell Ni@Sno_2 composites with a designable interspace to improve the electromagnetic wave absorption properties," *ACS Appl. Mater. Interfaces*, vol. 8, no. 42, pp. 28917–28925, 2016.
[45] S. Xie *et al.*, "Recent progress in electromagnetic wave absorption building materials," *J. Building Eng.*, vol. 27, Jan. 2020, Art. no. 100963.
[46] S. N. Kharkovsky, M. F. Akay, U. C. Hasar, and C. D. Atis, "Measurement and monitoring of microwave reflection and transmission properties of cement-based specimens," *IEEE Trans. Instrum. Meas.*, vol. 51, no. 6, pp. 1210–1218, Dec. 2002.
[47] I. Ismail *et al.*, "Effect of Mn and Zn doping on natural resonance frequency of strontium U-type hexaferrite and its performance as electromagnetic wave absorbers," *J. Alloys Compounds*, vol. 898, Mar. 2022, Art. no. 163246.

Ugur Cem Hasar (Member, IEEE) received the B.Sc. and M.Sc. degrees (Hons.) in electrical and electronics engineering from Cukurova University, Adana, Turkey, in 2000 and 2002, respectively, and the Ph.D. degree (Hons.) in electrical and computer engineering from State University of New York at Binghamton, Binghamton, NY, USA, in 2008.

Since 2017, he has been a full-time Professor with the Department of Electrical and Electronics Engineering, Gaziantep University, Gaziantep, Turkey. His main research interests include microwave nondestructive testing and evaluation, millimeter waves, THz frequencies, porous silicon-based sensors, and metamaterials.

Prof. Hasar was a recipient of the Outstanding Young Scientist Award in Electromagnetics of Leopold B. Felsen Fund, the Binghamton University Distinguished Dissertation Award, the Binghamton University Student Award for Excellence in Research, and the Science Academy's Young Scientist Award.

Necip Altay Eren received the Ph.D. degree from Gaziantep University, Gaziantep, Turkey, in 2021.

He is currently an Academician at the Department of Construction, Technical Sciences Vocational School, Gaziantep University. His research interests include geopolymer concrete, impact performance, self-compacting concretes, fiber-reinforced alkali-activated materials, mechanical strength, and durability of geopolymers. He has published four SCI articles in these areas, and those received 18 citations.

Hamdullah Ozturk received the B.Sc. degree from the Department of Electrical and Electronics Engineering, University of Atılım, Ankara, Turkey, in 2015, and the M.Sc. degree from the Department of Electrical and Electronics Engineering, Iskenderun Technical University, Hatay, Turkey, in 2018. He is currently pursuing the Ph.D. degree with the Department of Electrical and Electronics Engineering, Gaziantep University, Gaziantep, Turkey.

His current research interests include the characterization of materials by microwave sensors and antennas.

Mucahit Izginli received the B.Sc. degree from the Department of Electrical and Electronics Engineering, Gaziantep University, Gaziantep, Turkey, in 2018, where he is currently pursuing the M.Sc. degree.

Since 2020, he has been working as a Research Assistant with the Department of Electrical and Electronics Engineering, Hasan Kalyoncu University, Gaziantep. His current research interests include the characterization of materials by microwave sensors and antennas.

Huseyin Korkmaz received the B.Sc. and M.Sc degrees in electrical and electronics engineering from Gaziantep University, Gaziantep, Turkey, in 2016 and 2019, respectively, where he is currently pursuing the Ph.D. degree with the Department of Electromagnetic Fields and Microwave Technique and the Department of Electrical and Electronics Engineering.

His research interests include micro and nano technology, photovoltaic solar cells, metamaterial-based absorbers, MXene, characterization of metamaterials at microwave frequencies, and adulteration detection of some liquids.

Abdulkadir Cevik is currently a Professor Doctor with the Department of Civil Engineering, Gaziantep University, Gaziantep, Turkey. He has published over 120 peer-reviewed research articles and books in these areas and received over 2600 citations. His research interests are soft computing, RC structures, steel structures, alkali-activated materials, artificial intelligence, impact performance, bond strength, fiber-reinforced alkali-activated materials, and mechanical strength and durability of geopolymers. Also, he has graduated more than 25 M.Sc. and Ph.D. students.

Prof. Cevik serves as a reviewer for the national and international journals.

Anil Nis is currently an Associate Professor with the Department of Civil Engineering, Istanbul Gelisim University, Istanbul, Turkey. He studies fiber-reinforced concretes, self-compacting concretes, mechanical strength, and durability of alkali-activated materials. He has published over 30 peer-reviewed research articles in these areas, including a book chapter and over 20 SCI-indexed articles that received more than 400 citations.

Prof. Nis also serves as an Assistant Editor for the *International Journal of Engineering Technologies* and serves as a Reviewer for international journals, including *Construction and Building Materials*, *Cleaner Engineering and Technology*, *Journal of Building Engineering*, *Advances in Concrete Construction*, and *Case Studies in Construction Materials*.

Mohammad R. Irshidat received the bachelor's and master's degrees (Hons.) in civil engineering from the Jordan University of Science and Technology (JUST), Irbid, Jordan, in 2004 and 2006, respectively, and the Ph.D. degree in civil engineering from the University of Mississippi, Oxford, MS, USA, in 2010.

He is currently the Director of the Center for Advanced Materials, Qatar University (QU), Doha, Qatar. He has a successful record of publications in refereed academic journals, peer-reviewed conference proceedings, and academic conference presentations. He has an active research agenda with collaborative projects with colleagues at Qatar University and other international universities. His research interests mainly focus on applied research projects in the field of sustainable construction materials, 3-D printable concrete, nanotechnology applications in structural engineering, and strengthening and rehabilitation of reinforced concrete structures.